Paper 1

Mesospheric temperatures derived from three decades of hydroxyl airglow measurements from Longyearbyen, Svalbard (78°N)

Holmen, S. E., M. E. Dyrland and F. Sigernes

Published in Acta Geophysica, 62 (2), 302–315, doi: 10.2478/s11600-013-0159-4, 2013.

VERSITA

Acta Geophysica
DOI: 10.2478/s11600-013-0159-4

Mesospheric Temperatures Derived from Three Decades of Hydroxyl Airglow Measurements from Longyearbyen, Svalbard (78°N)

Silje E. HOLMEN[1,2,3], Margit E. DYRLAND[1,2], and Fred SIGERNES[1,2]

[1]The University Centre in Svalbard, Longyearbyen, Norway
e-mails: siljeh@unis.no (corresponding author), margitd@unis.no, freds@unis.no

[2]Birkeland Centre for Space Science, Bergen, Norway

[3]University of Tromsø – The Arctic University of Norway,
Tromsø Geophysical Observatory, Tromsø, Norway

A b s t r a c t

The airglow hydroxyl temperature record from Longyearbyen, Svalbard, is updated with data from the last seven seasons (2005/2006-2011/2012). The temperatures are derived from ground-based spectral measurements of the hydroxyl airglow layer, which ranges from 76 to 90 km height. The overall daily average mesospheric temperature for the whole temperature record is 206 K. This is by 3 K less than what Dyrland and Sigernes (2007) reported in their last update on the temperature series. This temperature difference is due to cold winter seasons from 2008 to 2010. 2009/2010 was the coldest winter season ever recorded over Longyearbyen, with a seasonal average of 185 K. Temperature variability within the winter seasons is investigated, and the temperature difference between late December (local minimum) and late January (local maximum) is approximately 8 K.

Key words: airglow, mesosphere, Arctic, temperature, hydroxyl.

1. INTRODUCTION

The mesosphere and lower thermosphere (MLT) region is a part of the atmosphere characterized by strong variability in winter temperatures. Break-

ing of tidal, planetary and gravity waves in the MLT region controls the large-scale circulation and hence actuates vertical motion leading to adiabatic heating/cooling (Becker 2012). The dynamic connections between wave activity and temperature variability are particularly obvious during sudden stratospheric warmings (SSWs). In major SSW events, the polar vortex breaks down and the zonal-mean zonal winds reverse from westerly to easterly, and the stratosphere warms by up to 60 K very rapidly (Matsuno 1971, Walterscheid *et al.* 2000, Cho *et al.* 2004, Liu and Roble 2002). SSWs are confirmed through several studies to have a strong impact on fluctuations in the mesospheric airglow layers and hence mesospheric temperatures (Walterscheid *et al.* 1994). Solar flux variability is also believed to have an influence on the thermodynamics of the mesosphere, but the relationship between mesospheric temperature and the 27-day and 11-year solar cycles is still not fully understood (Beig *et al.* 2012, Matthes *et al.* 2004).

The ground-based spectral measurement of hydroxyl (OH) airglow from Longyearbyen, Svalbard, started in 1980. The derived rotational temperature series is one of the longest continuous winter records in the world. Sigernes *et al.* (2003) and Dyrland and Sigernes (2007) have earlier reported on trends and features in the temperature series from Longyearbyen. Also other studies have been carried out on the OH* temperatures from Longyearbyen, with focus mainly on tidal and seasonal variations and the influence of SSWs and gravity waves (Myrabø 1984, Nielsen *et al.* 2002, Dyrland *et al.* 2010). Myrabø (1986) reported to have identified a seasonal pattern in winter with relatively low temperatures in late December followed by higher temperatures in January. Diurnal and semi-diurnal variations in the dataset have also been analysed, with results varying from a 13 K semi-diurnal amplitude found (Walterscheid *et al.* 1986) to no considerable periods identified (Dyrland and Sigernes 2007).

This study, with the supplement of OH* airglow derived temperatures from the last seven winter seasons, gives an update on the mesospheric winter temperature series from Longyearbyen, Svalbard. The OH* airglow temperatures are presented and discussed in connection with SSWs and wave activity. The spectral measurement technique is described in Section 2. The results are presented and discussed in Section 3. Section 4 is a summary of the results.

2. DATA AND MEASUREMENT TECHNIQUE

In this study, OH*(6-2) airglow rotational temperatures are derived from the 1 m focal length Ebert–Fastie spectrometer located in Longyearbyen. The temperatures are weighted averages from the height range of the vibrational state of OH*(6-2). According to Mulligan *et al.* (2009), the peak altitude of

the OH layer ranges from 76 to 90 km. The observing season is from the beginning of November to the end of February.

The Ebert–Fastie spectrometer was placed in the Auroral Station in Adventdalen (78°N, 15°E) in 1983, but it was moved to the new station, the Kjell Henriksen Observatory (KHO) on the mountain Breinosa (78°N, 16°E) in 2007. The distance between the two sites is approximately 8 km. The field of view of the instrument is 5 degrees in the zenith direction. The cone angle is slightly larger in the direction parallel to the entrance slit. At 90 km altitude the latter corresponds to a measurement area of $\sim 9 \times 12$ km. The move of the instrument should therefore have no impact on the comparability of the time series when it comes to the measurement area. However, the local weather conditions above the two different sites and contamination by artificial light sources may be slightly different. The potential impact on the derived temperatures will be discussed further in Section 3.1.

The rotational temperatures are derived from the measured spectra by calculating synthetic spectra as a function of instrumental bandpass and temperature. Then the background is detected by finding the optimal fit between the measured and synthetic spectra. The temperatures are derived from the slope of a linear fit to a Boltzmann plot using $P_1(2)$, $P_1(3)$, $P_1(4)$, and $P_1(5)$ rotational line intensities of the OH*(6-2) band. Energy term values are taken from Krassovsky *et al.* (1962), and Einstein coefficients are from Mies (1974). The basis for the calculation of the spectra is given by Herzberg (1950).

Some of the spectra are contaminated by aurora or by scattering of moonlight by clouds. To sort out contaminated spectra, the covariance between synthetic and measured spectra is calculated. A poor fit between the measured and the synthetic spectra is either caused by a very high background intensity or by occurrence of the auroral OI 8446 Å emission line, which is located close to the $P_2(4)$ line of the OH*(6-2) band. The fit variance of P_1 and P_2 is also calculated for every spectrum in order to ensure local thermal equilibrium. Spectra with covariance between measured and synthetic spectra less than 0.8 are discarded. This is also the case for spectra with P_1 fit variance greater than 0.05 and P_2 fit variance greater than 0.3. For further details on the instrument and the temperature retrieval method, see Sigernes *et al.* (2003) and Dyrland and Sigernes (2007). An example of a synthetic fit to an hourly averaged measured spectrum from 7 January 2012 at 19 UTC is shown in Fig. 1.

Viereck and Deehr (1989) considered the above method to have an uncertainty of approximately ± 5 K for 15 minute average temperature retrievals. For the more recent data the uncertainties have been calculated for each hourly averaged spectra from the error in the least squares fit of the Boltzmann plot. The error in the daily averaged temperature has been calculated

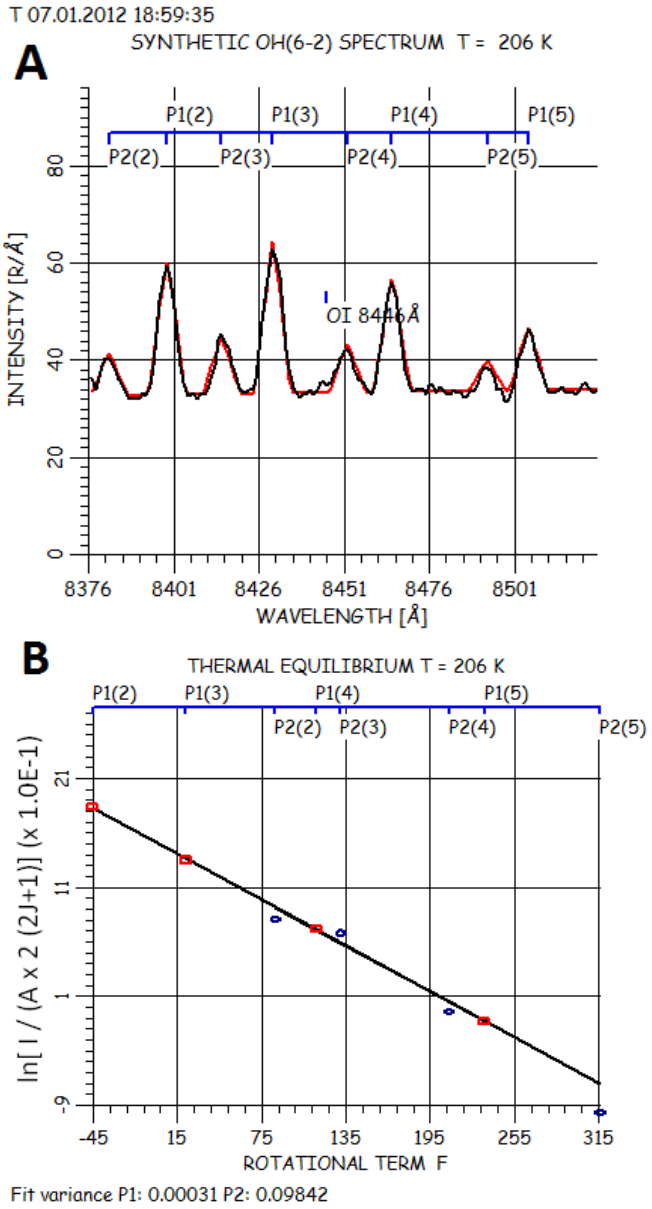

Fig. 1. Panel A shows the synthetic fit to an hourly averaged measured spectrum from 7 January 2012 at 19 UTC. The red curve is the measured spectrum, and the black curve is the synthetic, fitted spectrum. During this hour there was no contamination of the averaged spectrum due to the auroral OI 8446 Å emission line, as can be seen from the very good fit between the two curves. Panel B shows the corresponding Boltzmann plot to the spectrum in panel A. The straight line is the linear fit using P_1 and P_2 values. A spread of the P_2 values from the linear fit would indicate a departure from thermal equilibrium. For this particular spectrum the covariance, P_1 fit variance and P_2 fit variance were 0.99, 0.0003, and 0.1, respectively. Colour version of this figure is available in electronic edition only.

by weighting the hourly averaged temperatures according to their individual uncertainty following the method of Bevington and Robinson (1992). The errors of the daily averaged temperatures range between 0.2-5 K.

3. RESULTS AND DISCUSSION

3.1 Seasons 2005/2006-2011/2012

In Fig. 2 daily averaged temperatures retrieved from the OH* airglow layer over Longyearbyen are presented. Daily averages of temperatures are estimated for days with three or more hours of data that satisfy the covariance and fit variance criteria mentioned in Section 2. Together with the OH* temperatures, 10 hPa stratospheric temperature is plotted. The 10 hPa temperature is a NASA reanalysis temperature provided through the Modern-Era Retrospective analysis for Research and Applications (MERRA) project (NASA 2012).

From Fig. 2 we see that the data coverage over the seven winter seasons analysed is variable, but especially the 2010/2011 and 2011/2012 winters have very good data coverage. The reason is partly that the photomultiplier tube (PMT) of the instrument was changed in January 2011, providing a better signal-to-noise ratio that allowed more spectra to be analysed, and partly the varying weather conditions of the different seasons. The move of the in-

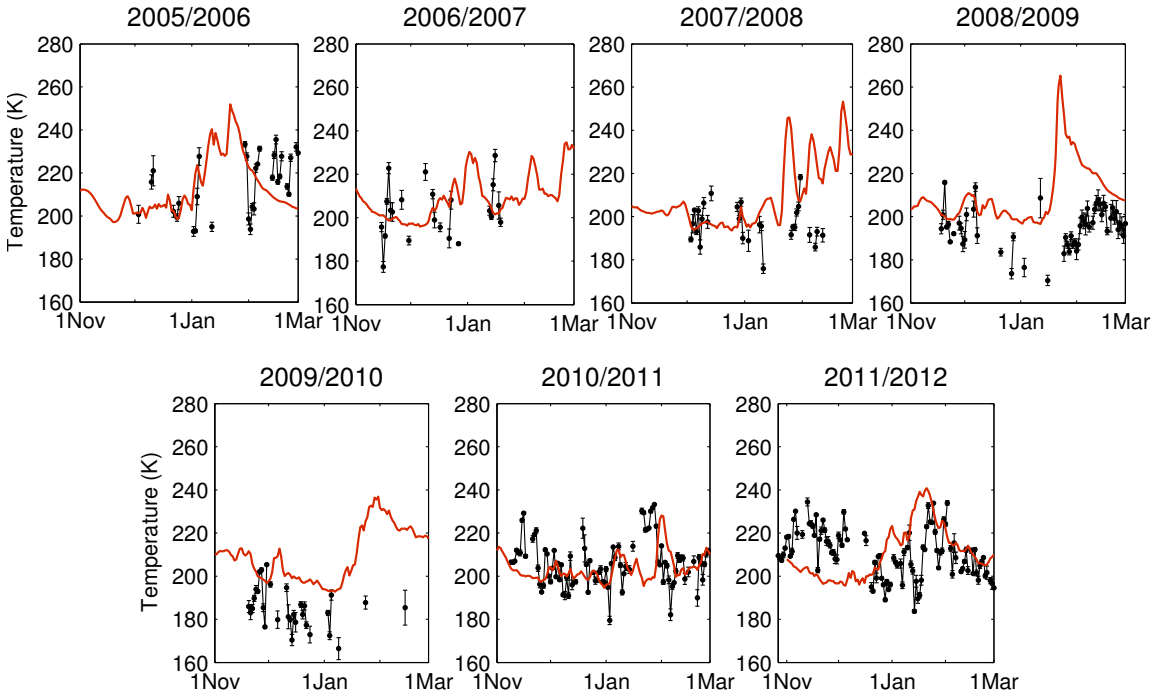

Fig. 2. Daily averaged temperatures retrieved from OH*(6-2) airglow emissions over Longyearbyen, Svalbard, for the winter seasons of 2005/2006 through 2011/2012. The OH* temperatures are plotted as black bullets with ± 1 standard deviation indicated as errorbars. The 10 hPa stratospheric MERRA temperatures are plotted as red lines. The OH* temperatures are weighted averages from 76 to 90 km, while the 10 hPa MERRA temperatures are at about 30 km in the stratosphere and vary by a few km depending on the synoptic meteorological conditions. Colour version of this figure is available in electronic edition only.

strument itself in 2007 may also have contributed to an increase in data points. Contamination from artificial light from the town is much less at the KHO compared to the old Auroral Station because of the larger distance to the town. In addition, there is significantly less light contamination from snowmobiles and cars. No official cloud cover statistics for the two sites exists, so it is hard to draw categorical conclusions about the local differences. It is however possible that there may be some local differences in cloud cover that would bring a bias to the temperatures, but this difference is here assumed to be small.

The seven seasons reported here appear to some extent to agree with a hypothesis that some SSWs are preceded by a cooling seen in OH* temperatures a few days earlier, which is reported earlier in literature (Hoffmann *et al.* 2007, Walterscheid *et al.* 2000). We see that an increase in stratospheric temperature (red line) sometimes succeeds a decrease in OH* temperatures, but this is hard to confirm to a full extent because of the lack of data for some periods.

It must be noted that a change in OH* temperature may be due to either a temperature change in the height distribution of OH*(6-2), a change in the height distribution itself, or a combination of both (Baker and Stair 1988, Mulligan *et al.* 2009).

The average temperature, standard deviation and maximum and minimum temperatures of all seven seasons are listed in Table 1. We see that the standard deviation in general is higher in January compared to December. A reason for this may be a higher occurrence of SSWs and planetary wave activity in late winter (January–March) (Labitzke and Naujokat 2000, Kuttippurath and Nikulin 2012), which again is a source of high variability in OH* temperatures.

Table 1

Average, maximum, and minimum temperatures, including standard deviations, for seasons 2005/2006 through 2011/2012

Winter season	Number of days	Mean *T* Nov-Feb [K]	Mean *T* Dec [K]	Mean *T* Jan [K]	Max *T* [K]	Min *T* [K]
2005/2006	31	215 ± 13	208 ± 8	211 ± 17	236	193
2006/2007	22	203 ± 12	202 ± 11	208 ± 11	229	177
2007/2008	28	197 ± 9	199 ± 7	196 ± 10	218	176
2008/2009	54	195 ± 9	193 ± 12	187 ± 10	216	170
2009/2010	30	185 ± 9	182 ± 7	180 ± 9	205	166
2010/2011	93	206 ± 11	201 ± 7	212 ± 13	233	180
2011/2012	103	211 ± 11	207 ± 12	210 ± 13	234	184

Note: In addition to the average over the whole winter season from November through February, the average for December and January is listed.

Occasionally, the OH* temperatures increase very rapidly over a relatively short time period. This is especially noticeable in January 2012, when the temperature increases by approximately 50 K in just a couple of days. This takes place during a minor SSW. These kind of fluctuations in the OH* airglow are most likely due to propagation and breaking of planetary and gravity waves in the mesosphere, as reported in literature (Sivjee *et al.* 1987, Hoffmann *et al.* 2007).

3.2 The updated temperature series 1983-2012

In Fig. 3 annual averaged airglow temperatures from the 1983/1984 through the 2011/2012 seasons are presented. Only seasons with ten or more daily averaged temperatures calculated have been included in the plot. The seasonal average is the average of December and January temperatures. Missing values for the 1990/1991, 1991/1992, 1992/1993, 1993/1994, 1996/1997, and 1998/1999 seasons can either be explained by too few temperatures retrieved or by instrument problems.

The average temperature for the whole temperature series is 206 K, when using Einstein coefficients from Mies (1974). This is by 3 K less than what was found in the previous work done on the time series by Dyrland and Sigernes (2007) on the period from 1983 to 2005. The maximum temperature of the temperature record is 253 K (19 February 2004) and the minimum temperature is 166 K (9 January 2010). We see from Fig. 2 that some of the latest years analysed are quite cold years, especially the 2008/2009 and the 2009/2010 seasons. This is in accordance with recent publications from other

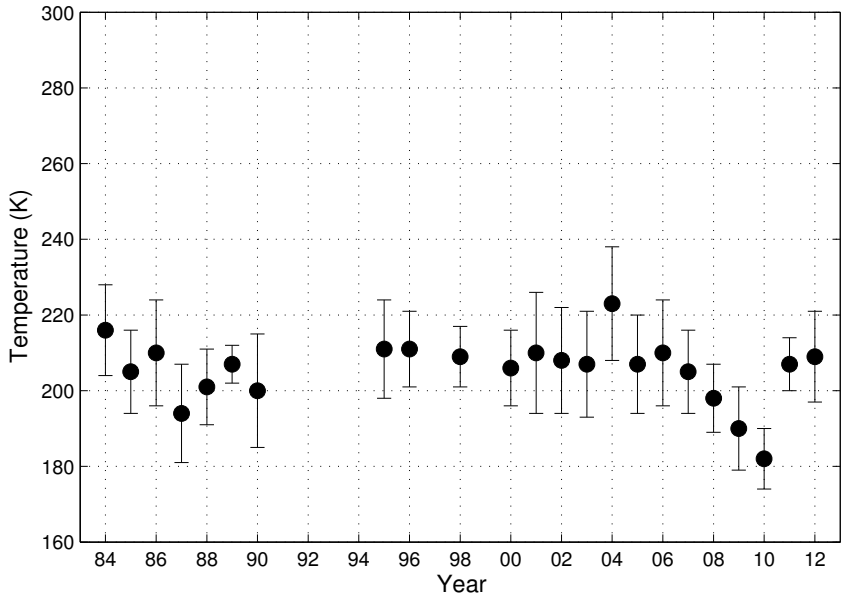

Fig. 3. Seasonal averages of OH* rotational temperatures from Longyearbyen, Svalbard, 1983-2012, plotted as black bullets with the standard deviation as errorbars.

locations (French and Klekociuk 2011, Offermann *et al.* 2010). This may partly be explained by that during the last decade, an increasing number of SSWs have been detected compared to the 1990s. Kuttippurath and Nikulin (2012) investigated the major SSWs in the Arctic observed between 2003/2004 and 2009/2010, and found that the SSW in the 2008/2009 season was the strongest. Even though the stratosphere was relatively cold in the first part of the 2009/2010 winter season, this season experienced the largest momentum flux of all seasons. This took place in the end of January and beginning of February.

Temperature variations within the winter season were examined by superposing all OH* temperatures by day of year and then applying a 5-day running mean on the superposed temperatures. This is the same method as that described in French and Klekociuk (2011) and Azeem *et al.* (2007). The superposed temperatures are shown in Fig. 4. The black lines represent ± 1 standard deviation, the red line represents the 5-day running mean, and the blue line represents a 15-day running mean. We see from the lines representing running means that there are some variations in temperature within the winter season. There are local temperature maxima in late January and in February, while there is a local minimum in the end of December / beginning of February. The local temperature minimum in late December / early January is consistent with what Myrabø (1986) found for the winter seasons in the first part of the 1980s in Longyearbyen. The temperature difference between late December and late January is approximately 8 K when looking at

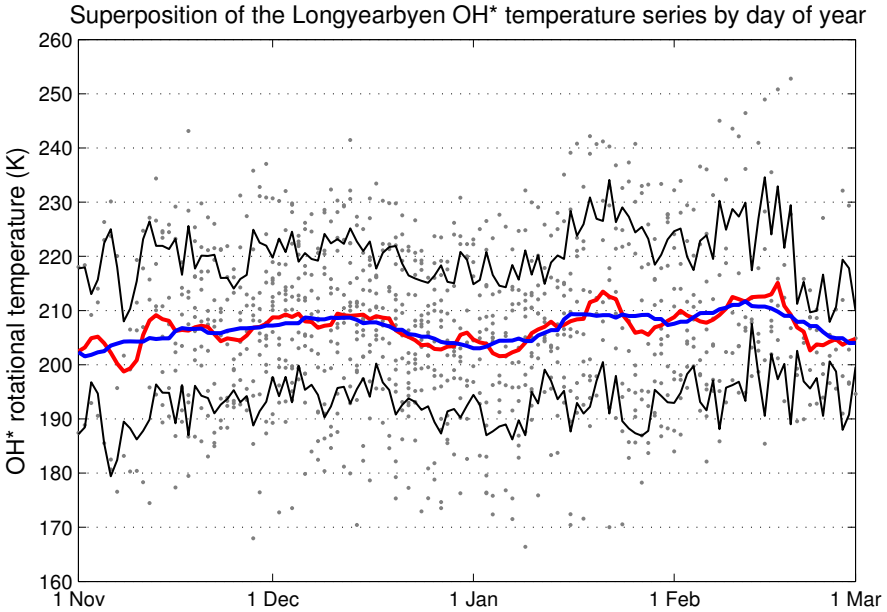

Fig. 4. Superposition of the Longearbyen OH* temperatures by day of year. Grey dots are the daily averaged OH* temperatures, and the black lines represent ± 1 SD. The red line is the 5-day running mean, and the blue line is the 15-day running mean. Colour version of this figure is available in electronic edition only.

the 5-day running mean. This is in accordance with the climatology Hall *et al.* (2012) reported for Svalbard using temperatures from the Nippon / Norway Svalbard Meteor Radar (NSMR) located in Adventdalen near Longyearbyen.

As mentioned for Fig. 2, the OH* temperatures used in Fig. 4 may be influenced not only by the temperature change within the height range, but also by a change in height of the OH* layer.

The overall standard deviation of the Longyearbyen hydroxyl temperature record is 15 K. This is higher than the standard deviations estimated for other locations (*e.g.*, French and Klekociuk 2011, Bittner *et al.* 2002). The reason for this is not completely clear, but one explanation may be that the mountainous topography in Svalbard favours gravity wave formation and thus great variability in temperatures. However, when looking at two high-latitude stations in Antarctica, the Davis and the Amundsen–Scott South Pole stations, these also experience substantial gravity wave activity (Beldon and Mitchell 2009, Collins *et al.* 1994). This occurs even though the standard deviations are reported to be significantly lower than for Longyearbyen. An explanation for some of the variability in temperatures may be the weather regimes. Especially the South Pole station is rarely hit by heavy storms, which are characteristic for Antarctic coastal areas. Also, there are in general less clouds above this station compared to over Longyearbyen (Town *et al.* 2007, eKlima 2012). Longyearbyen is frequently hit by strong low pressure systems, which makes the weather during the winter season unstable. This may result in higher standard deviations.

Mies was the first to calculate Einstein coefficients for hydroxyl vibration-rotation bands in 1974 (Mies 1974). Since then, several updates have been published in order to improve temperature estimates, *e.g.*, Turnbull and Lowe (1989), Goldman *et al.* (1998), and Van der Loo and Groenenboom (2007). Even though more recent updates on the Einstein coefficients exist, the coefficients from Mies (1974) were used in this study. This was done in order to compare the temperatures obtained from the seven winter seasons analysed with the temperatures obtained from 1983 to 2005. The use of different Einstein coefficients is considered to have a significant impact on the estimated temperatures. Perminov *et al.* (2007) state that the use of different Einstein coefficients may give differences in temperatures as high as 5-14 K. Several studies have been carried out during the last decade to determine which Einstein coefficients give the most accurate temperatures, and there is no general agreement about this matter (French *et al.* 2000, Pendleton and Taylor 2002, Cosby and Slanger 2007). It is important to have this in mind when looking at the absolute temperatures.

An updated trend of the Longyearbyen temperature record is not presented in this paper. A thorough analysis and discussion about the trend with

regard to seasonal variations and solar cycle dependence will be published in a future paper.

4. CONCLUSIONS

The OH*(6-2) airglow temperature record from Longyearbyen, Svalbard (78°N, 16°E) is updated with data from the winter seasons of 2005/2006 through 2011/2012. The data coverage of these seven seasons is variable, but the 2010/2011 and 2011/2012 seasons have excellent data coverage. We see that a decrease in OH* temperatures is to some extent followed by an increase in stratospheric temperatures during SSW events.

The variability in airglow temperatures over Longyearbyen is very high, both on a day-to-day basis and within a season. In some periods, OH* temperatures can increase or decrease by 30-50 K in just a couple of days. The standard deviations of each season range from 9 to 13 K. This is significantly higher than standard deviations reported from other locations. The reason for this is not fully understood, but one explanation may be that the topography around Longyearbyen favours gravity wave activity, which again is a known contributor to variability in mesospheric temperatures. Also weather systems in the Arctic, and thus unstable observing conditions, may explain temperature variability.

When looking at the whole temperature record from 1983 to 2012, the overall average temperature is 206 K, by 3 K less than what Dyrland and Sigernes (2007) reported for their update on the temperature record. It is noticeable that some of the most recent winter seasons were very cold. Especially the 2009/2010 season was cold, with a seasonal average of 185 K and a daily averaged minimum of 166 K measured on 9 January 2010. This is the lowest daily temperature of the whole temperature record. The low temperatures for the years 2008-2010 are in accordance with temperatures reported from other locations and with the fact that strong SSWs took place during that time.

There are monthly temperature variations within the winter season. The data show local temperature maxima in late January and in February, while there is a local minimum in the end of December / beginning of February. The temperature difference between late December and late January is approximately 8 K.

Acknowledgments. This work was financially supported by The Research Council of Norway through the projects named: Norwegian and Russian Upper Atmosphere Co-operation On Svalbard part 2 # 196173 / S30 (NORUSCA2), Infrastructure for Space Physics Related Research on Svalbard # 195385 (INFRASPACE) and High-Arctic Gravity waves and their impact on middle atmospheric circulation and temperature (# 204993).

References

Azeem, S.M.I., G.G. Sivjee, Y.-I. Won, and C. Mutiso (2007), Solar cycle signature and secular long-term trend in OH airglow temperature observations at South Pole, Antarctica, *J. Geophys. Res.* **112**, A1, A01305, DOI: 10.1029/2005JA011475.

Baker, D.J., and A.T. Stair Jr. (1988), Rocket measurements of the altitude distributions of the hydroxyl airglow, *Phys. Scr.* **37**, 4, 611, DOI: 10.1088/0031-8949/37/4/021.

Becker, E. (2012), Dynamical control of the middle atmosphere, *Space Sci. Rev.* **168**, 1-4, 283-314, DOI: 10.1007/s11214-011-9841-5.

Beig, G., S. Fadnavis, H. Schmidt, and G.P. Brasseur (2012), Inter-comparison of 11-year solar cycle response in mesospheric ozone and temperature obtained by HALOE satellite data and HAMMONIA model, *J. Geophys. Res.* **117**, D4, D00P10, DOI: 10.1029/2011JD015697.

Beldon, C.L., and N.J. Mitchell (2009), Gravity waves in the mesopause region observed by meteor radar. 2: Climatologies of gravity waves in the Antarctic and Arctic, *J. Atmos. Solar-Terr. Phys*. **71**, 8-9, 875-884, DOI: 10.1016/j.jastp.2009.03.009.

Bevington, P.R., and D.K. Robinson (1992), *Data Reduction and Error Analysis for the Physical Sciences*, McGraw-Hill, New York, 328 pp.

Bittner, M., D. Offermann, H.-H. Graef, M. Donner, and K. Hamilton (2002), An 18-year time series of OH rotational temperatures and middle atmosphere decadal variations, *J. Atmos. Solar-Terr. Phys*. **64**, 8-11, 1147-1166, DOI: 10.1016/S1364-6826(02)00065-2.

Cho, Y.-M., G.G. Shepherd, Y.-I. Won, S. Sargoytchev, S. Brown, and B. Solheim (2004), MLT cooling during stratospheric warming events, *Geophys. Res. Lett.* **31**, 10, L10104, DOI: 10.1029/2004GL019552.

Collins, R.L., A. Nomura, and C.S. Gardner (1994), Gravity waves in the upper mesosphere over Antarctica: Lidar observations at the South Pole and Syowa, *J. Geophys. Res.* **99**, D3, 5475-5485, DOI: 10.1029/93JD03276.

Cosby, P.C., and T.G. Slanger (2007), OH spectroscopy and chemistry investigated with astronomical sky spectra, *Can. J. Phys*. **85**, 2, 77-99, DOI: 10.1139/p06-088.

Dyrland, M.E., and F. Sigernes (2007), An update on the hydroxyl airglow temperature record from the Auroral Station in Adventdalen, Svalbard (1980-2005), *Can. J. Phys*. **85**, 2, 143-151, DOI: 10.1139/p07-040.

Dyrland, M.E., F.J. Mulligan, C.M. Hall, F. Sigernes, M. Tsutsumi, and C.S. Deehr (2010), Response of OH airglow temperatures to neutral air dynamics at 78°N, 16°E during the anomalous 2003-2004 winter, *J. Geophys. Res.* **115**, D7, D07103, DOI: 10.1029/2009JD012726.

eKlima (2012), Norwegian Meteorological Institute's climate database, http://eklima.met.no/, accessed November 2012.

French, W.J.R., and A.R. Klekociuk (2011), Long-term trends in Antarctic winter hydroxyl temperatures, *J. Geophys. Res.* **116**, D4, D00P09, DOI: 10.1029/2011JD015731.

French, W.J.R, G.B. Burns, K. Finlayson, P.A. Greet, R.P. Lowe, and P.F.B. Williams (2000), Hydroxyl (6-2) airglow emission intensity ratios for rotational temperature determination, *Ann. Geophys*. **18**, 10, 1293-1303, DOI: 10.1007/s00585-000-1293-2.

Goldman, A., W.G. Schoenfeld, D. Goorvitch, C. Chackerian Jr., H. Dothe, F. Mélen, M.C. Abrams, and J.E.A. Selby (1998), Updated line parameters for OH $X^2\Pi$-$X^2\Pi$ (v″,v′) transitions, *J. Quant. Spectrosc. Radiat. Transfer* **59**, 3-5, 453-469, DOI: 10.1016/S0022-4073(97)00112-X.

Hall, C.M., M.E. Dyrland, M. Tsutsumi, and F.J. Mulligan (2012), Temperature trends at 90 km over Svalbard, Norway (78°N 16°E), seen in one decade of meteor radar observations, *J. Geophys. Res.* **117**, D8, D08104, DOI: 10.1029/2011JD017028.

Herzberg, G. (1950), *Molecular Spectra and Molecular Structure. Vol. I. Spectra of Diatomic Molecules*, Van Nostrand Company Inc., New York.

Hoffmann, P., W. Singer, D. Keuer, W.K. Hocking, M. Kunze, and Y. Murayama (2007), Latitudinal and longitudinal variability of mesospheric winds and temperatures during stratospheric warming events, *J. Atmos. Solar-Terr. Phys*. **69**, 17-18, 2355-2366, DOI: 10.1016/j.jastp.2007.06.010.

Krassovsky, V.I., N.N. Shefov, and V.I. Yarin (1962), Atlas of the airglow spectrum 3000-12 400 Å, *Planet. Space Sci*. **9**, 12, 883-915, DOI: 10.1016/0032-0633(62)90008-9.

Kuttippurath, J., and G. Nikulin (2012), A comparative study of the major sudden stratospheric warmings in the Arctic winters 2003/2004-2009/2010, *Atmos. Chem. Phys*. **12**, 17, 8115-8129, DOI: 10.5194/acp-12-8115-2012.

Labitzke, K., and B. Naujokat (2000), The lower Arctic stratosphere in winter since 1952, *SPARC Newsletter* **15**, 11-14.

Liu, H.-L, and R.G. Roble (2002), A study of a self-generated stratospheric sudden warming and its mesospheric-lower thermospheric impacts using the coupled TIME-GCM/CCM3, *J. Geophys. Res.* **107**, D23, 4695, DOI: 10.1029/2001JD001533.

Matsuno, T. (1971), A dynamical model of the stratospheric sudden warming, *J. Atmos. Sci.* **28**, 8, 1479-1494, DOI: 10.1175/1520-0469(1971)028<1479:ADMOTS>2.0.CO;2.

Matthes, K., U. Langematz, L.L. Gray, K. Kodera, and K. Labitzke (2004), Improved 11-year solar signal in the Freie Universität Berlin Climate Middle Atmosphere Model (FUB-CMAM), *J. Geophys. Res.* **109**, D6, D06101, DOI: 10.1029/2003JD004012.

Mies, F.H. (1974), Calculated vibrational transition probabilities of OH($X^2\Pi$), *J. Mol. Spectrosc.* **53**, 2, 150-188, DOI: 10.1016/0022-2852(74)90125-8.

Mulligan, F.J., M.E. Dyrland, F. Sigernes, and C.S. Deehr (2009), Inferring hydroxyl layer peak heights from ground-based measurements of OH(6-2) band integrated emission rate at Longyearbyen (78°N, 16°E), *Ann. Geophys.* **27**, 11, 4197-4205, DOI: 10.5194/angeo-27-4197-2009.

Myrabø, H.K. (1984), Temperature variation at mesopause levels during winter solstice at 78°N, *Planet. Space Sci.* **32**, 2, 249-255, DOI: 10.1016/0032-0633(84)90159-4.

Myrabø, H.K. (1986), Winter-season mesopause and lower thermosphere temperatures in the northern polar region, *Planet. Space Sci*. **34**, 11, 1023-1029, DOI: 10.1016/0032-0633(86) 90012-7.

NASA (2012), Annual Meteorological Statistics, National Aeronautics Space Administration, http://acdb-ext.gsfc.nasa.gov/Data_services/met/ann_data.html, accessed October 2012.

Nielsen, K.P., F. Sigernes, E. Raustein, and C.S. Deehr (2002), The 20-year change of the Svalbard OH-temperatures, *Phys. Chem. Earth* **27**, 6-8, 555-561, DOI: 10.1016/S1474-7065(02)00037-2.

Offermann, D., P. Hoffmann, P. Knieling, R. Koppmann, J. Oberheide, and W. Steinbrecht (2010), Long-term trends and solar cycle variations of mesospheric temperature and dynamics, *J. Geophys. Res.* **115**, D18, D18127, DOI: 10.1029/2009JD013363.

Pendleton Jr., W.R., and M.J. Taylor (2002), The impact of *L*-uncoupling on Einstein coefficients for the OH Meinel (6,2) band: implications for *Q*-branch rotational temperatures, *J. Atmos. Solar-Terr. Phys*. **64**, 8-11, 971-983, DOI: 10.1016/S1364-6826(02)00051-2.

Perminov, V.I., A.I. Semenov, and N.N. Shefov (2007), On rotational temperature of the hydroxyl emission, *Geomag. Aeron*. **47**, 6, 756-763, DOI: 10.1134/S0016793207060084.

Sigernes, F., N. Shumilov, C.S. Deehr, K.P. Nielsen, T. Svenøe, and O. Havnes (2003), Hydroxyl rotational temperature record from the auroral station in Adventdalen, Svalbard (78°N, 15°E), *J. Geophys. Res.* **108**, A9, 1342, DOI: 10.1029/2001JA009023.

Sivjee, G.G., R.L. Walterscheid, J.H. Hecht, R.M. Hamwey, G. Schubert, and A.B. Christensen (1987), Effects of atmospheric disturbances on polar mesopause airglow OH emissions, *J. Geophys. Res.* **92**, A7, 7651-7656, DOI: 10.1029/JA092iA07p07651.

Town, M.S., V.P. Walden, and S.G. Warren (2007), Cloud cover over the South Pole from visual observations, satellite retrievals, and surface-based infrared radiation measurements, *J. Climate* **20**, 3, 544-559, DOI: 10.1175/JCLI4005.1.

Turnbull, D.N., and R.P. Lowe (1989), New hydroxyl transition probabilities and their importance in airglow studies, *Planet. Space Sci*. **37**, 6, 723-738, DOI: 10.1016/0032-0633(89)90042-1.

Van der Loo, M.P., and G.C. Groenenboom (2007), Theoretical transition probabilities for the OH Meinel system, *J. Chem. Phys*. **126**, 11, 114314-1-114314-7, DOI: 10.1063/1.2646859.

Viereck, R.A., and C.S. Deehr (1989), On the interaction between gravity waves and the OH Meinel (6-2) and the O_2 atmospheric (0-1) bands in the polar night airglow, *J. Geophys. Res.* **94**, A5, 5397-5404, DOI: 10.1029/JA094iA05p05397.

Walterscheid, R.L., G.G. Sivjee, G. Schubert, and R.M. Hamwey (1986), Large-amplitude semidiurnal temperature variations in the polar mesopause: evidence of a pseudotide, *Nature* **324**, 7445, 347-349, DOI: 10.1038/324347a0.

Walterscheid, R.L., G. Schubert, and M.P. Hickey (1994), Comparison of theories for gravity wave induced fluctuations in airglow emissions, *J. Geophys. Res.* **99**, A3, 3935-3944, DOI: 10.1029/93JA03312.

Walterscheid, R.L., G.G. Sivjee, and R.G. Roble (2000), Mesospheric and lower thermospheric manifestations of a stratospheric warming event over Eureka, Canada (80°N), *Geophys. Res. Lett*. **27**, 18, 2897-2900, DOI: 10.1029/2000GL003768.

Received 23 November 2012
Received in revised form 20 March 2013
Accepted 18 April 2013